Satellite Constellation Mission Design using Model-Based Systems Engineering and Observing System Simulation Experiments

Sreeja Nag
Massachusetts Institute of Technology
77 Massachusetts Avenue, Cambridge, MA 02139; 617-710-1845
sreeja_n@mit.edu

Faculty Advisor: Prof. Olivier de Weck
Massachusetts Institute of Technology

ABSTRACT

Distributed Space Missions (DSMs) are gaining momentum in their application to earth science missions owing to their unique ability to increase observation sampling in spatial, spectral, angular and temporal dimensions simultaneously. Since DSM architectures are defined by monolithic architecture variables and variables associated with the distributed framework, they have many and often conflicting design variables and objectives. There are very few open-access tools available to explore the tradespace of variables, minimize cost and maximize performance for pre-defined science goals, and therefore select the most optimal constellation design. This paper presents a software tool, developed on the MATLAB engine interfaced with STK, that is based on tightly coupled science and engineering models. It can generate hundreds of DSM architectures based on pre-defined design variable ranges and size those architectures in terms of pre-defined science and cost metrics. The tool's performance analysis module is driven by the concept of observing system simulation experiments (OSSE), traditionally used to validate proposed instruments. The architecture and simulated measurement generation is driven by Model-Based Systems Engineering (MBSE). The utility of the tool is demonstrated using a case study to determine the Earth's global, diurnal Radiation budget more accurately than current monolithic instruments.

BACKGROUND – CONTELLATION MISSION DESIGN

Distributed Space Missions (DSMs) are gaining momentum in their application to earth science missions owing to their ability to simultaneously increase observation sampling in spatial, spectral, temporal and angular dimensions. DSMs encompass a diverse family of spacecraft configurations including homogenous constellations such as GPS and Iridium, heterogeneous constellations such as the A-Train, close proximity clusters in active formation flight such as the upcoming Proba-3 and fractionated spacecraft where all physical entities share subsystem functions such as System F6[1]. DSMs may be deployed in a staged fashion[2], reconfigurable while in orbit and replenished when older satellites enabling graceful degradation[3]. This allows for scalability, flexibility and evolvability in the mission and puts less pressure on risks and schedule. Technologies to support DSMs have also seen a great increase: Proximity operations and formation flight, orbit initialization and scatter maneuvers [4], high data rate communication links, miniaturized thrusters for active control and open-source cluster flight development[5]. While on-orbit demonstrations have been few, the advent of new technologies point to an optimistic future for DSM demonstrations for improved science.

Since DSM design and operation is a function of a much larger number of variables than its monolithic counterparts as well as have higher costs, it is imperative to understand the trade-offs and interdependencies among the variables early in the design stage. Model-Based Systems Engineering (MBSE) has demonstrated success in small satellite design[6] in trading conflicting design variables and is a useful tool for pre-Phase A DSM design.

In the traditional sense, observing system simulation experiments (OSSE) are used to quantify the impact of observations from future observation systems such as satellite instruments or ground-based networks on e.g. weather forecasts, by mimicking the process of data assimilation. In atmospheric applications, real imperfect observations are drawn from the real atmosphere (data or model) to produce estimates of global atmospheric states at sequences of time. For land applications, simulated land surface states are propagated through the sensor measurement and retrieval process to investigate

and constrain expected levels of retrieval error. The goal is to validate science return for proposed instruments and therefore the instrument design.

A tradespace of constellation designs can be analyzed by varying the design variables in the MBSE model and assessing its effect on data assimilation and science products using OSSEs. This paper introduces a *general methodology and software tool* that applies this analysis approach to constellation and formation flight for earth observation. Candidate science products are photosynthetic efficiency, albedo, leaf area indices, normalized difference vegetation indices, etc. As a *candidate case study*, the methodology will be applied to global radiation budget estimations for the Earth.

CASE STUDY - EARTH RADIATION BUDGET ESTIMATION

Earth Radiation Imbalance (ERI), which is the difference between the Total Solar Irradiance divided by 4 (TSI/4) and Total Outgoing Radiation (TOR), is estimated to be 0.9 W/m^2 by current climate models (annual average) with an uncertainty between -2 and +7 W/m^2 [7,8]. In fact, there is uncertainty even about the uncertainty: models and observations pin it at 0.5 W/m^2 [9,10] while oceanographers sat 0.4 to 0.7 W/m^2 [11]. Since climate change results from a less than 1% ERI and TSI is estimated at 341.3W/m^2 [11] with 0.03% accuracy, there is great scientific need to improve the estimation accuracies of TOR. If the Earth had no internal processes such as winds and clouds, the ERI would radiated out by Plank's Law, however the their presence causes radiative forcing and possible entrapment of heat. Reference [12] and [10] have shown that the Earth's energy budget is not closed which means that there is a large portion of ERI that is not being absorbed as heat by the oceans (Figure 1 blue region).

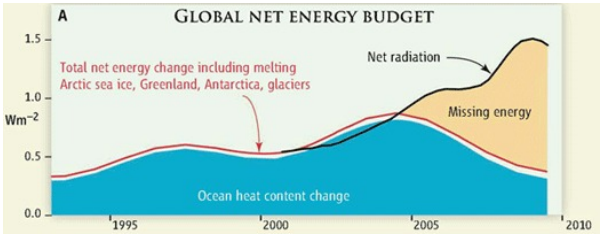

Figure 1: Missing energy between ocean heat content and ERI observations as shown in [10]

Traditional assumptions ignore short time scale radiative forcing (<1 month) such as the diurnal cycle and the intra-seasonal time scales such as the Madden Julien oscillations, but scientists have argued that forcing in one scale can influence long term climate. For example, the net flux measured by the CERES instrument [13] on TERRA and AQUA in morning and afternoon sun synchronous orbits respectively has been monotonically increasing over the years [7]. Thus, nonlinear analysis of ERI time record with global and high temporal sampling, without assuming or approximating Gaussian distributions is needed [14]. NOAA specified accuracy for future ERB measurements is 1.7 W/m^2 for total channel and 1 W/m^2 for shortwave, with radiometric stability of 0.3 W/m^2. Up to 90% of the errors in the computation of atmospheric radiative forcing, which is a key assessor of climate change, is attributed to the lack of good angular description of reflected solar flux[15]. Previous studies have also suggested the use of the quadrature sampling technique by multiple satellites to reduce errors in radiative forcing estimation [16,17].

Johns Hopkins University's Applied Physics Lab (JHU APL) is currently developing a cubesat radiometer called RAVAN (Radiometer Assessment using Vertically Aligned Nanotubes), due for flight demonstration in 2015. RAVAN is a low cost, compact, NIST-standard instrument that uses vertically aligned carbon nanotube (VACNT) absorbers and has a flux resolution better than 0.3 W/m^2, as required by the ERI. It will be a wide field of view (FOV ~ 130 deg), broadband radiometer. A constellation of RAVANs are potentially provide a dense sampling of TOR and capture its global and temporal (especially the diurnal cycles) variation. Initial results have simulated the performance of such radiometers on the 66 Iridium NEXT satellites and shown its success using 66 satellites[18]. Dependencies on integration time (2 hours vs. 3 hours) of the flux played an important role in the results as did the number of satellites.

This paper builds on prior work by assessing the dependency of ERB performance on different constellation and orbit variables and instrument fields of view, and therefore finding the Pareto number of satellites required for capturing the *temporal, global and angular variation* of the ERB.

PROPOSED METHODOLOGY

The optimal constellation configuration is one that minimizes the TOR measurement errors with respect to true TOR as well as minimizes cost, i.e. demonstrates Pareto optimality [19]. A tradespace analysis, sofware tool has been developed that achieves this objective by combining the MBSE approach with the OSSE approach. The tool enumerates dozens of architectures with different combinations of the following design variables: altitude, inclination, number of satellites, number of planes, instrument field of view and constellation type (e.g. streets of coverage vs. Walker Delta). Altitude-inclination combinations, as available

for easy commercial launches, and variables that affect science, such as integration time for TOR, can be considered. The tool has previously been applied to formation flight design for angular reflectance measurements to estimate bi-directional reflectance distribution functions[20,21]. For compactness, only constellation orbits will be discussed in this paper.

The high level structure of the tool, shown in Figure 2, is essentially a coupled systems engineering model (quantified by an N2 diagram representing the key design variables arranged by subsystems) and science evaluation model. The SysEng model – driven by MBSE - generates the architectures and simulates measurements over the mission period. The measurements are then evaluated by the SciEval model – driven by OSSE. Technology specifics, cost and science performance are outputs for each architecture and are used to make an informed selection of the final design.

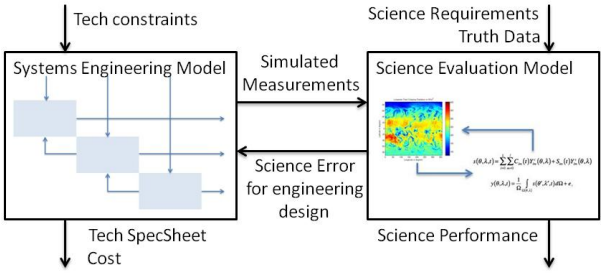

Figure 2: Tradespace Analysis Tool overview. The Science Evaluation Model (right box) is modeled after the OSSE concept and tightly coupled to the traditional MBSE module (left box).

The SysEng model been developed on MATLAB. For the purpose of compactness, only the orbits module of the MBSE tool is presented in this paper. The MATLAB engine is used to drive AGI's Systems Toolkit to generate customized constellations by varying design parameters as shown in Figure 3. Figure 5 Box2 shows an example of a constellation architecture. Reports are generated for temporal and angular coverage for every grid point on the Earth and every time point in the analysis time period, for every architecture. Some examples of reports are the measurement zenith angle of access and access duration. These reports are then post-processed to output customized figures of merit depending on the science application. For example, some temporal performance metrics, shown in Figure 3, are average revisit time and percent global coverage.

Each architecture's goodness is evaluated using the SciEval model shown in Figure 4 and cost calculated based on the design variables[22]. The SysModel outputs simulated measurements per architecture (Box2), which serve as the input to the "OSSE". These measurements determine the subset of the true TOR (Box1) that the constellation's sensors can 'see'. Samples of the true TOR are selected accordingly (Box3) and a model is fit on the samples to estimate model parameters (Box 4). The next section discusses the potential models, especially the spherical harmonics model, that can be used for this purpose. The inverted model parameters are used to determine TOR globally, over time (Box 6) and compared to the truth (Box 1) to give an objective measure of goodness of the architecture with respect to the UMGLO model truth (Box1). The Pareto optimal architectures are then selected as a function of the two objective metrics: performance error and cost.

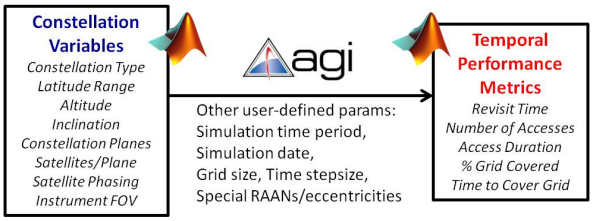

Figure 3: Constellation design variables and their mapping to some example metrics.

Some components of the tool will be discussed below in context of the case study with the intention of showing how the methodology works. Measurement integration methods, science models and truth data will depend on the application under consideration. Both the methodology and the software tool are modular enough to allow easy swapping of case studies.

Flux Integration over Instrument FOV

The critical measurement estimating step is the integration of the radiance "seen" by the instrument over its FOV. Assuming the instrument aperture to be a polygon of area dA, as seen in Figure 4 (left), the total flux reaching it is the integration of the infinitesimal cones of radiance coming from multiple, radiating grid points on the Earth (in the Ω direction). The area of each element of the Earth grid can be calculated from its equivalent spherical polygons and thus subtends a calculable angle δω at the aperture. Alternatively, δω may be converted into (θ,φ) coordinates as seen in Figure 4 (right). Total flux (hemispheric) is then given by the radiance integration of δω over FOV:

$$Flux = \int_{2\pi} Radiance(\Omega)cos(\theta)d\omega = \int_0^{2\pi}\int_0^{\pi/2} Radiance(\theta,\varphi)cos(\theta)sin(\theta)d\theta d\phi$$

Equation 1

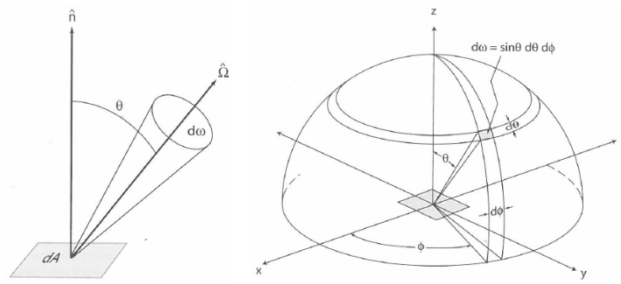

Figure 4: Spherical Geometry representation of radiance and TOR at the satellite

Science Models – Simple Averaging and Spherical Harmonics

The main purpose of a science model is to estimate the measurements at all points in space and time, given a sample set of measurements at a subset of those space-time points. Compressed sensing theory suggests the use of spherical harmonics (SH) to theoretically model radiation leaving a sphere[23] and the measurements are suggested to be the convolution of the images formed using independent sources. The SH model provides a way to synthesize, from a discrete sample on a sphere, the complete distribution on the entire sphere. The first harmonic coefficient finds the total mean outgoing flux on a sphere, while other higher degree harmonics represent the detail structures of spatial distribution. Reconstruction may incorporate prior information.

Spherical harmonics based reconstruction has been used for evaluating the geopotential of the Earth in the GRACE mission[24]. The GRACE mission bears a qualitative similarity to the ERB mission, in that it represents a mathematical field, the geopotential, on the surface of a sphere [25]. In the SH model, TOR (s(θ,λ,t) – in Equation 2) is expressed at the satellite altitude, location in latitude/longitude and time using a truncated SH model. The basis functions are $Y^c_{lm}(\theta,\lambda) = P_{lm}(cos\theta)cos(\mathrm{m}\lambda)$, $Y^s_{lm}(\theta,\lambda) = P_{lm}(cos\theta)sin(\mathrm{m}\lambda)$, where $P_{lm}(cos\theta)$ is the associated Lengendre polynomial, θ and λ are latitude and longitude respectively. The onboard radiometer will measure the spatially-averaged TOR (instead of in situ TOR) over the instrument field-of-view and yield a spatially integrated measurement y(θ,λ,t) in Equation 2 with some e as measurement noise.

$$s(\theta,\lambda,t) = \sum_{l=0}^{L}\sum_{m=0}^{l} C_{lm}(t)Y^c_{lm}(\theta,\lambda) + S_{lm}(t)Y^s_{lm}(\theta,\lambda)$$

$$y(\theta,\lambda,t) = \frac{1}{\Omega}\int_{\Omega(\theta,\lambda)} s(\theta',\lambda',t)d\Omega + e$$

$$y(\theta,\lambda,t) = \sum_{l=0}^{L}\sum_{m=0}^{l}\left[\bar{C}_{lm}\bar{Y}^c_{lm}(\theta,\lambda) + \bar{S}_{lm}\bar{Y}^s_{lm}(\theta,\lambda)\right] + e$$

Equation 2

Combining the two equations gives the simulated measurements, y(θ,λ,t), as a function of the basis functions whose coefficients can be solved for if a sufficient number of satellite measurements of flux are available and the satellite position (θ,λ) is known.

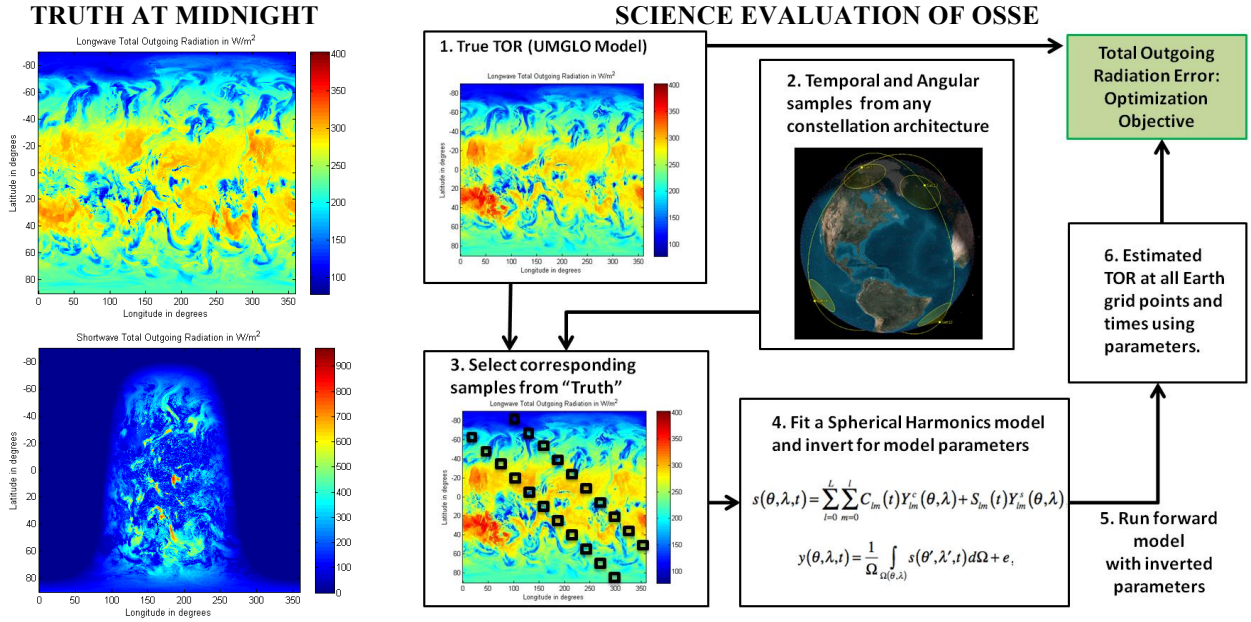

Figure 5: [Left] TOR at every grid point on Earth at 00:00 on August 29, 2010, as generated by the modified UMGLO model for longwave (top) and shortwave (bottom) radiation. Such data is available and used as truth at 3 hour intervals. [Right] Process flow chart for evaluating the 'goodness' of any constellation architecture (Box 2) in terms of the objective of minimizing the TOR error (green box).

The two sets of harmonic coefficients, C/S and $\bar{C}/\bar{S}$ are related by the Pellican cap parameter, β in Equation 3, which acts as a smoothening filter over the true data[26]. Larger FOVs will result in smoother measured fluxes because harmonics from neighboring points will affect the measurements.

$$\begin{Bmatrix}\bar{C}\\ \bar{S}\end{Bmatrix} = \beta_l \begin{Bmatrix}C\\ S\end{Bmatrix}$$

$$\beta_l = \frac{1}{1-\cos FOV}\frac{1}{l+1}[P_{l-1}(\cos FOV) - \cos FOV\, P_l(\cos FOV)]$$

$$\beta_1 = \frac{1}{2}\left[\sin FOV \cot\frac{FOV}{2}\right] \quad \beta_0 = 1$$

Equation 3

The averaged coefficients can be inverted from measurements and the true coefficients estimated from them analytically. Flux at any latitude and longitude on the sphere can then be calculated from the true coefficients. Figure 6 shows the difference in true TOR at the Equator and estimated TOR using the above method in 1D for varying FOV and for different density of measurements. Denser measurements result in lesser errors. Measurements at 24 deg apart i.e. 15 near-simultaneous measurements result in <1W/m^2 of difference from the truth, which is the NOAA prescribed accuracy for shortwave retrievals. When measurements are not well spread, errors soar even if their numbers are large. Figure 6's right most bars show 48 measurements simulated over 24 deg of the Equator resulting in the maximum error. Therefore, it is not just the measurement and satellite numbers, but also the spread and arrangement that is very important. Higher FOVs reduce error for uniform spread because of more overlap and ability to capture angular variation of the true data but increase error for clustered spread.

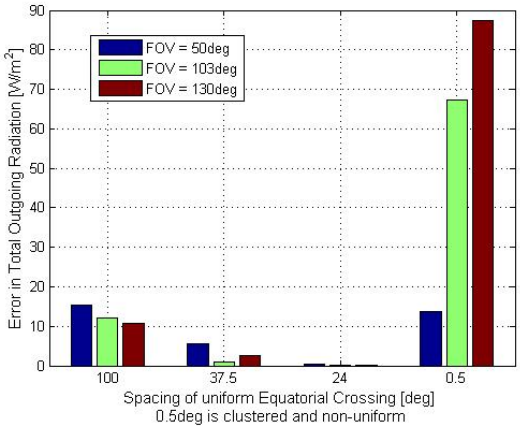

Figure 6: Difference in true and estimated TOR using 1D spherical harmonics for equally spaced measurements along the Equator (left 3 sets) and clustered measurements over 24^o (right set), i.e. 3, 9, 15 uniform and 48 clustered measurements.

TOR is assumed to be static over three hours, validated by climate science models. The spatial resolution of the proposed SH model is the Earth circumference divided by the number of SH terms in the expansion - "l" in Equation 2. Therefore, more model parameters and more satellites are required for more spatial resolution (e.g. 100 for a 400 km resolution). Measurements are very high look angles/nadir angles are also noisier (high e), so just increasing the field of view per satellite is not sufficient. Increasing FOV also averages out the truth and misses angular dependence of radiance, requiring more satellites and more overlap to converge to the true flux. This creates a strong case for constellations.

Truth Data – UMGLO Model and CAR Data

Truth data for OSSE can be obtained from prior campaigns of the same geographic areas of interest such as tower measurements of radiance from plants or airborne measurements of reflectance of snow. The ERB case study requires TOR globally and bi- or tri-hourly. Since such measurements have never been obtained, a global climate model is used along with a radiative transfer model to generate the TOR at every 0.3516 deg of longitude and 0.2344 deg of latitude, every three hours through August 29, 2010 (arbitrarily selected). The Met Office global forecast model[27] (UMGLO) is used to generate the TOR data. Assuming the UMGLO radiation field to be isotropic, radiance is equal in all directions of the outgoing flux hemisphere.

$$Radiance = Flux/\pi$$

Equation 4

In practice, however, earth reflectance in the solar spectrum is anisotropic and is quantified by the Bi-Directional Reflectance Distribution Function (BRDF). BRDF of an optically thick body is a property of the surface material and its roughness. It is the ratio of reflected radiance to incident irradiance that depends on 3D geometry of incident and reflected elementary beams. Solar reflectance can be represented as BRDF(θ,Θ,φ,λ), or the reflectance at a given solar zenith angle Θ, measurement zenith angle θ, relative azimuth between the two directions φ, at a specific wavelength λ.

$$Radiance = BRDF(\theta, \Theta, \varphi, \lambda) * Flux$$

Equation 5

BRDF values for six of the major biomes of the Earth are available from airborne campaigns and have been used to quantify the anisotropy of the radiation field output from the UMGLO model. Data from the Cloud Absorption Radiometer (CAR) instrument[29], developed at NASA Goddard Space Flight Center (GSFC), quantifies reflectance at all 4 BRDF variables, θ,Θ,φ,λ

at an instrument FOV of 1 deg and over 14 bands from 335 to 2344 nm. Since this paper focuses on broadband, wide FOV measurements, CAR measurements can be averaged to provide the same. For example, Figure 7 shows the reflectance or BRDF of Arctic snow as an example (averaged over all wavelengths but constant solar zenith) for varying measurement zenith and azimuth. Measured flux over snow when BRDF is accounted for is 45%-50% higher than when only nadir reflectance is considered. Since a large amount of TOR is reflected off the polar ice, BRDF considerations are important to estimate the truth correctly.

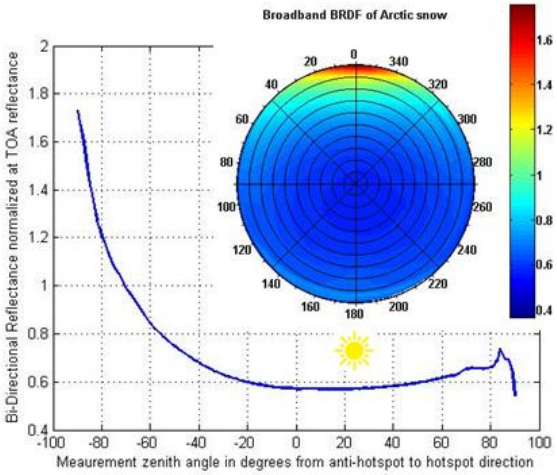

Figure 7: BRDF of Arctic snow[28], as an example. Blue curve-broadband reflectance of snow measured by CAR, normalized at the top of the atmosphere (TOA) measured in the vertical plane containing the sun and target. Polar plot- broadband reflectance of snow at all measurement zenith angles (θ=radius) and relative azimuth with respect to the Sun (Φ=polar azimuth). Solar zenith Θ = 67 deg.

Cost Model

The cost of the Theoretical First Unit (TFU) is assumed to be that spent on developing and flight-testing the RAVAN instrument on the APL cubesat. The constellation cost will be a function of this TFU and the learning curve to build multiple copies. Cost to copy is defined as the cost of a copy as a percentage of TFU. Due to learning curve effects, cost to copy decreases as the number of manufactured copies (N-1) increases.
Studies at JHU APL started with cost to copy factor of 35% [30,31], performed regression analysis on Juno JEDI (N=3), RBSPICE (N=2), STEREO (N=2) and Van Allen Probes (N=2) and validated a cost copy factor of 30-40% for their engineering practices [32]. They published the cost to copy (C2C) to be 28%, 45%, 41% and 36% respectively [32] for the above 4 instruments. Assuming that JEDI and RBSPICE were all copies of each other [32], the C2C for 2, 3 and 5 units was found. Using this published data and assuming an initial learning curve factor (b=85%), I fit the learning equation (Equation 6) to the data. The estimated learning parameter for APL is found to be b = 66.2% [22]. This value will be applied to cost multiple spacecrafts in a constellation. Learning curves are applied only the recurring fractions of the TFU cost. Recurring fractions are obtained from reference [33], for example ground station support is 0 and IAT is 1. Non-recurring costs are estimated by regular multiplication of units.

$$RE_{total} = \left(RE_{payload} + RE_{bus}\right) * N * N^{\log b / \log 2}$$

Equation 6

APPLICATION TO THE CASE STUDY

The proposed MBSE-OSSE coupled methodology and software tool is applied to the ERB constellation design case study. Initial results for a simple case with fixed altitude, inclination and FOV will be shown below. The altitude and inclination is chosen to be the same as TERRA and AQUA (709 km, 98.18 deg), because they house the CERES instrument – 2 copies - which has contributed significantly to the Earth Radiation Budget Experiment (ERBE) in the past decade. Since a lot of Earth Observation satellites such as LANDSAT are in the same altitude-inclination combination, commercial launches to the same will also be readily available. FOV is chosen to be 130 deg (for initial studies) in keeping with the current RAVAN design.

Architecture Generation and Technology Metrics

STK (without the Analyzer and parallel computing license) was found to be inefficient for tradespace exploration. Coverage for every point in the Earth grid has to be individually calculated for every satellite sensor in the constellation and for every angle required. Since the nadir pointing angle between the satellite location and the grid point is essential for computing radiance, the coverage reports took a couple of hours per satellite using the Grid Inspector tool. STK was thus only used for satellite propagation using the High Precision orbital Propagator (HPOP) with up to J4 effects. The satellite positions in latitude-longitude-altitude were saved for every time step. Grid points were also similarly saved as reports. Angular metrics for all accesses were calculated using post-processing. This new tool was validated against STK's angular reports and works 1500X times faster and results in <4 deg of angular errors for a 5 deg X 5 deg grid spacing.

The SysEng model was automated to generate 16 architectures with increasing number of satellites from 1 to 64 satellites arranged in different ways as constellations with maximum 8 planes and equal

satellites per plane. Near full and continuous global coverage is achieved using 32 satellites arranged in 4 planes with 8 satellites per plane as seen in Figure 8(a). When 32 satellites are arranged differently Figure 8(b), coverage is not continuous. The 64 satellite case allows a significantly overlapped coverage - Figure 8(c).

(a) 32 satellites = 4 planes X 8 satellites/plane

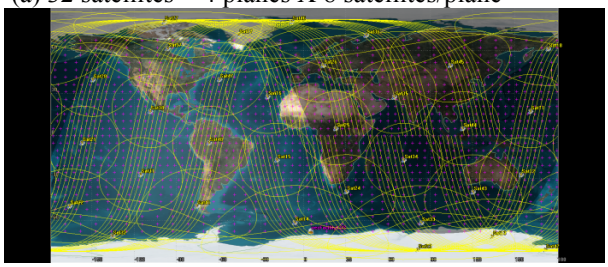

(b) 32 satellites = 8 planes X 4 satellites/plane

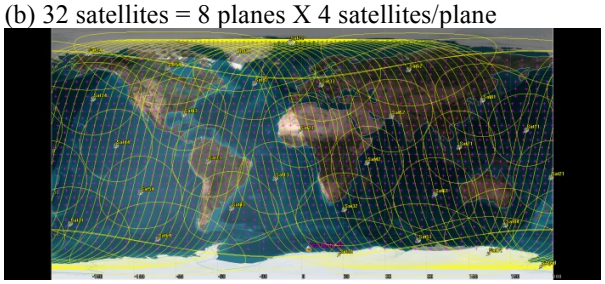

(c) 64 satellites = 8 planes X 8 satellites/plane

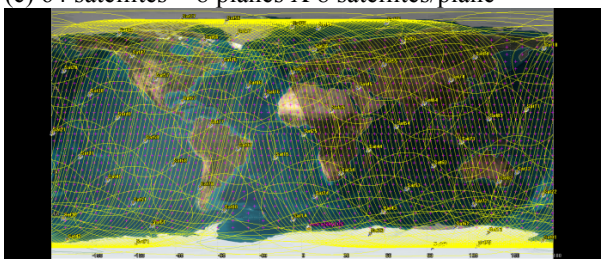

Figure 8: Examples of simulated Walker constellations at 709 km, 98.18 deg orbits with 130deg FOV instruments.

Since TOR is assumed to be static over 3 hours, an important result is to assess the grid points accessed and the extent of global coverage over a 3 hour time period. The OSSE tool is used to output and plot this information in Figure 9. Each colored curve represents a different architecture and shows the percentage of global coverage as a function of propagated time. All architectures with 8 satellites or more cover the full globe in less than three hours. The four satellite case (red) takes a little over 3 hours to do the same. The 64 satellite case (golden) is not seen on the chart because it provides near continuous coverage so global access takes only a few minutes.

Figure 9's results imply that for a 3 hour static TOR, any constellation with more than 8 satellites provides global and overlapping coverage. If TOR was assumed dynamic by the minute, overlapping coverage would require more than 32 satellites. Since measured TOR is averaged over the instrument FOV, more overlap decreases estimation error. It also shows the rate of global coverage for the CERES instrument on TERRA and AQUA (both given by the blue curve because they are monoliths) and the CERES instrument on the TRMM satellite (black curve). CERES has two modes of operation – a cross track scan which scans from limb to limb and an azimuthal scan. Clearly, monolithic coverage cannot capture less than 10-hour variations of TOR and have imprecise estimations at 24 hours as well because of the lack of overlapping observations. Since TRMM is on a 350 km/35 deg orbit, the maximum globe covered even after 24 hours is only 80% (65% within 10 hours) because it cannot access latitudes greater than 55 deg. Therefore, it is even more inaccurate for ERG global estimation. Each of the architectures described above are then quantified in terms of the time required by them to access every grid point on the Earth, as shown in Figure 10. In agreement with Figure 9, 32 satellites gives continuous coverage.

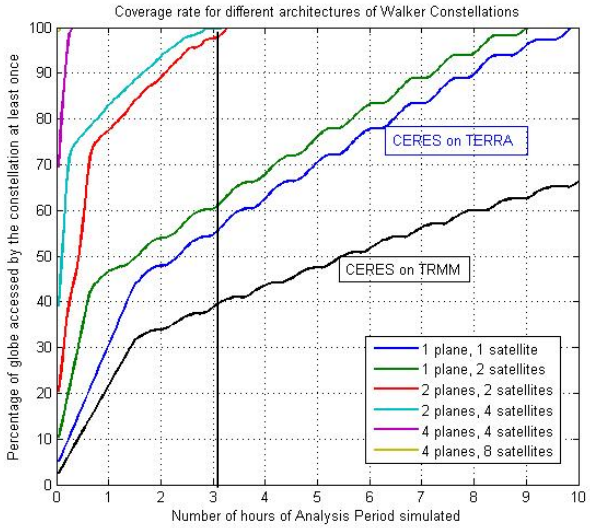

Figure 9: Time to global coverage per constellation architecture at 710 km, 98.18 deg and CERES

Since the chosen orbit 709 km/98.18 deg inclination is a 16 day repeat track orbit, an N satellite, evenly distributed constellation will result in an effective 16/N day repeat track. Therefore, every point will be revisited at exactly the same angle once a day in a 16 satellite constellation. The revisit interval, of course, will be much more frequent (~5 hours) due to the wide FOV of the instrument. The tradespace analysis tool has can easily output the average revisit times over the grid as well as individual revisit times per grid point, just as the previously demonstrated metric (time for global coverage). The modular framework allows more customized metrics to be easily incorporated.

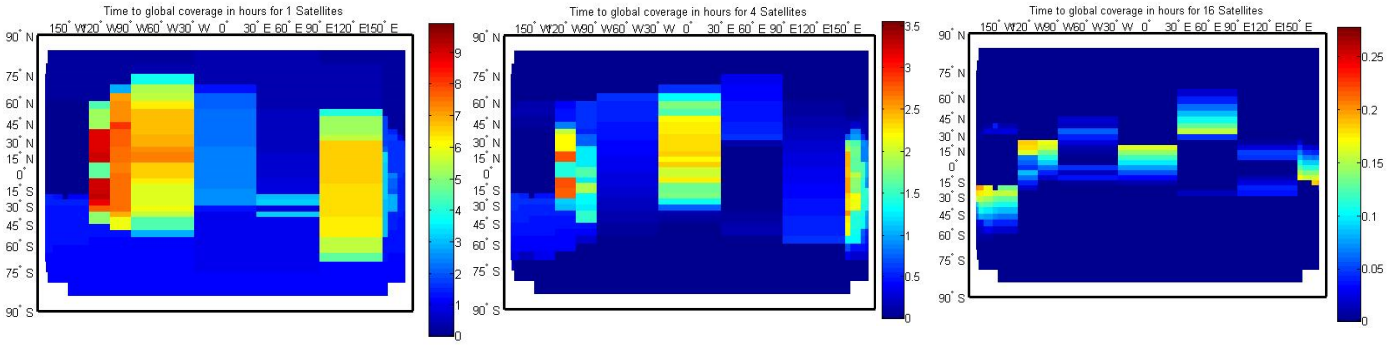

Figure 10: Time in hours required to access a grid point for the first time for a constellation at Altitude709 km, Inclination 98.18 deg, FOV 130 deg and varying number of satellites. 32 satellites gives continuous coverage, and reaches zero time at all points (all blue). The wide FOV swath is clearly visible.

Science Evaluation and Science Metrics

The access reports and angles to all the grid points for every satellite in every constellation were post-processed using the method in Figure 5 to calculate the corresponding errors with respect to the truth. For each satellite, the radiance (assumed isotropic in this section) from every grid point in its field of view were averaged to find simulated measurement of flux. Such measurements were then integrated over the 3 hour static window and the satellites using a simple averaging model and norm-1 calculated against truth.

The results for longwave and shortwave radiation, when isotropic truth from the original UMGLO model is used, are shown in Figure 11. Multiple scatter points for any N number of satellites is seen in Figure 11 because N satellites can be arranged in different ways in a uniform constellation. For example, there are 4 ways to arrange 8 satellites. The more even distributions offer more coverage and overlap and therefore provide slightly smaller errors. Both *short and long wave errors show significant improvement up to 16 satellites and then saturate*. This could be because more than 8 satellites provide global coverage every 3 hours (Figure 9&10) and, in the absence on unpredictable angular dependencies in the truth, full coverage is sufficient for radiance estimations. None of the errors reach the NOAA prescribed accuracy of 1 W/m^2 and 1.7 W/m^2 accuracy in short and longwave respectively, however *improve monolithic retrievals by up to 50%*. Longwave results in larger errors because it contributes to more global heat leaving the Earth because it is independent of sun conditions.

The science evaluation model, similar to above, is run for the CERES instrument (144 deg FOV) on the TRMM satellite (35 deg inclination). As expected from Figure 9 (24 hours for 80% coverage and 10 hours for 65% coverage), the corresponding flux errors with respect to the UMGLO model are: 15.37 W/m^2 for shortwave radiation and 34.31 W/m^2 for longwave radiation. As low as a two satellite constellation with RAVAN radiometers in a near-polar orbit, is able to improve those estimations five times as seen in Figure 11. This demonstrates the need for a high inclination orbit for the ERB mission and the effectiveness of constellations at those inclinations.

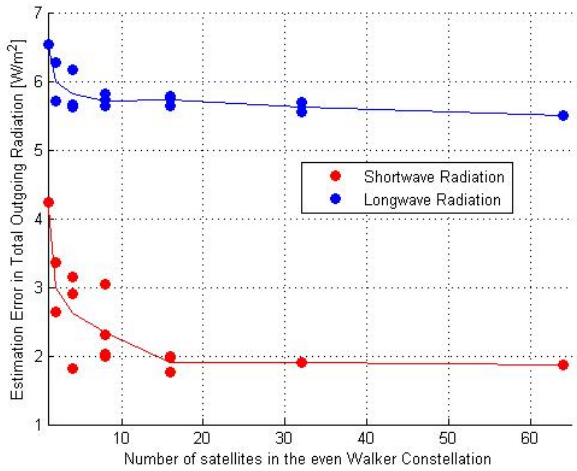

Figure 11: Norm-1 error of the TOR simulated measurements by an N-satellite Walker constellation (710 km) with respect to UMGLO mean flux, averaged globally and over one day. The horizontal black line indicates the NOAA required accuracy for ERB estimation.

Sensitivity to Constellation Orbits and Field of View

The developed software tool adhering to the coupled MBSE and OSSE methodology allows easy understanding of the science impact when one variable is changed. Coverage is primarily dependent on the ground spot in Earth degrees as plotted in ***Figure 12***. The minimum allowable inclination for global coverage

is 90 minus the ground spot. In the CERES example above, a 5 fold increase in TOR error was seen when the inclination was changed from 98.18 deg to 35 deg because the latter is not enough for global coverage at CERES ground spot. Considering commercial launches, the constellation is best launched into the TERRA (98.18 deg) or the Iridium inclination (86.4 deg).

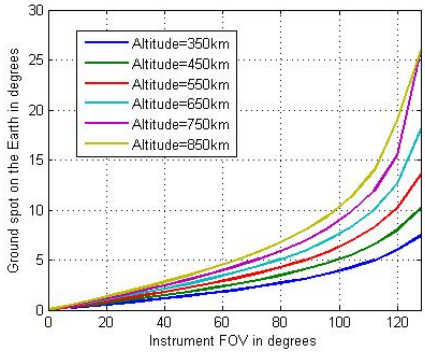

Figure 12: Ground spot size (main coverage metric) dependence on altitude and sensor field of view

Figure 12 shows that for a given ground spot and thus coverage, only one of altitude and FOV can be independently varied for non-redundant trades. The metric dependence on altitude for fixed FOV will be discussed below, but the insights are equally applicable for dependence on FOV for fixed altitude. Figure 13 shows the same constellation architecture as Figure 8(c) at a lower altitude of 500 km and lower coverage is apparent. At 500 km, simulations show that 8 planes X 16 satellites per plane = 128 satellites are required for continuous, global coverage. At 710 km, the same could be achieved with half the number of satellites. Assuming a 3 hour static TOR relaxes the satellite requirement by a margin. Figure 14 shows that the rate of global coverage curves have become significantly less steep compared to Figure 9. At 500 km, 16 satellites (red, 4 satellites in 4 planes) are required to achieve global coverage every three hours, almost twice the number required earlier. This clearly shows that a 200 km drop in constellation altitude requires twice the resources to achieve the same technical goals.

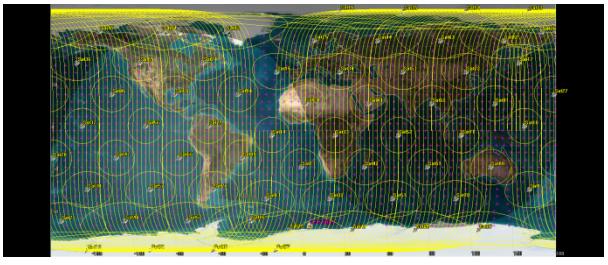

Figure 13: 64 satellite (8 plane X 8 satellites) Walker constellation at 500 km, 98.18 deg orbits with 130deg FOV instruments.

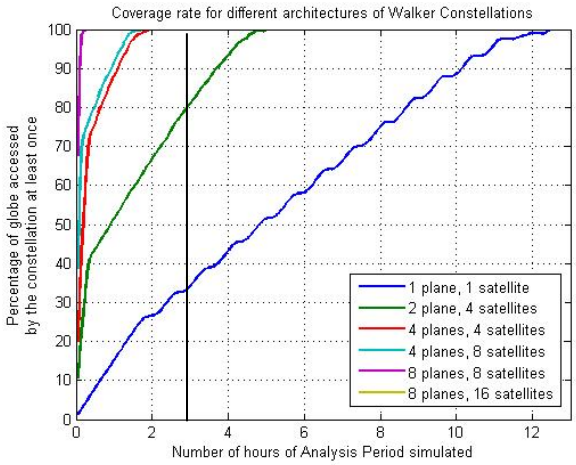

Figure 14: Time to global coverage per constellation architecture at 500 km, 98.18 deg and 130 deg FOV

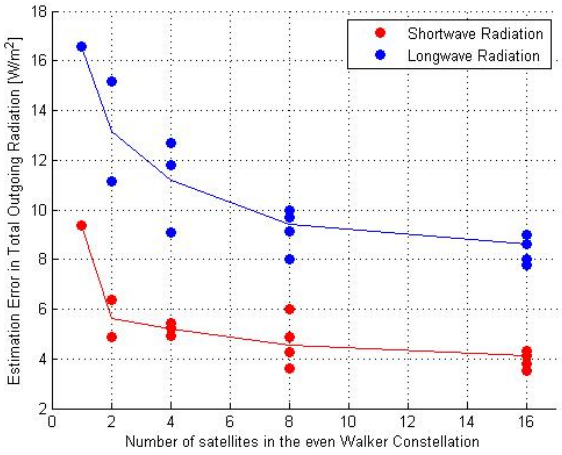

Figure 15: Norm-1 error of the TOR simulated measurements by an N-satellite Walker constellation (500 km) with respect to UMGLO mean flux, averaged globally and over one day.

The SciEval model outputs the TOR errors for the architectures generated above. Figure 15 shows a 1-2 fold increase in the TOR errors with respect to the UMGLO model compared to Figure 11. In other words, the same number of resources at a 200 km drop in altitude resulted *in less than double errors*. While the technical result above (*double satellites for same coverage*) is very informative, it is the TOR error values that speak more about the science impact to the mission. More satellites were not simulated because 16 satellites provide continuous coverage assuming 3-hour static TOR and, as seen before, the isotropic errors are expected to saturate even for more measurements. The SciEval model also shows that increasing the satellite numbers would likely not improve the errors at 500 km using the simple averaging model so *doubling*

resources may not halve the error and that there are constellation arrangements which can *produce lower errors with lower numbers of satellites.*

If altitude is raised, coverage will improve unless the ground spot already equals the Earth disc. Even so, the TOR errors need not improve because the simulated measurements will now include more grid points and more ground spot overlaps will be necessary to resolve them. It is such conflicting effects that demonstrate the indispensability of a coupled OSSE tool with the MBSE tool. Further, increasing the altitude more than 710 km will cause the Earth limb and beyond to be visible within the FOV. This will cause the *radiometer to be plagued by significant solar noise (sunblips)* when the sun is in its FOV. Signal to noise ratio during such events will be low and the measurements may not be useful.

Sensitivity to Anisotropy

The Earth radiation field is not isotropic, as assumed in the previous sections. The output flux of the UMGLO model is combined with the BRDF measurements made by the CAR during different NASA airborne campaigns using Equation 5 to generate an anisotropic truth field globally. Since CAR data is local and static, all grid points were sorted into land cover type from NASA's MODIS database and flux per grid point corrected using CAR reflectance for the appropriate biome. Only shortwave radiation is considered because BRDF is valid only in the near solar spectrum. Longwave radiation has a much milder angular dependence, especially for broadband applications (Limb darkening is seen in a few wavelengths only).

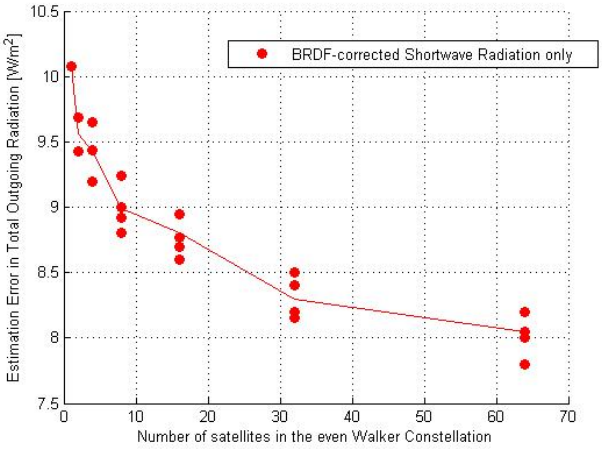

Figure 16: Norm-1 error of the TOR simulated by an N-satellite Walker constellation (710 km) with respect to UMGLO mean flux, corrected for anisotropy using the CAR airborne data set over MODIS land cover retrieved biomes.

Using an anisotropic data as truth, 25 architectures with satellite numbers from 1 through 64 were analyzed as before. Figure 16 shows the results of the analysis. Absolute errors nearly triple when compared to the isotropic results from Figure 11, because the architectures are unable to capture the unpredictable angular variation of true flux. However, the errors show continuous improvement even at 64 satellites because more ground spot overlap captures the angular dependence better. This demonstrates, as expected, that an *anisotropic radiation field requires more satellites* to achieve the same performance than isotropic radiation field because the angular variation of data needs to be captured along with the spatial and temporal variation.

Sensitivity to Science Models (Spherical Harmonics)

When the SH model is used to model the spatio-temporal spread of TOR and simulated measurements used to estimate its coefficients, the errors compared to truth improve significantly. Averaging over FOV and over a satellite's ground track over represent flux from ground points seen more than others, and do not necessarily show improved errors with improved FOV overlap. Using SH eliminates these biases by assuming and resolving flux as a functional representation, which is open to improvement using wavelets and other approaches.

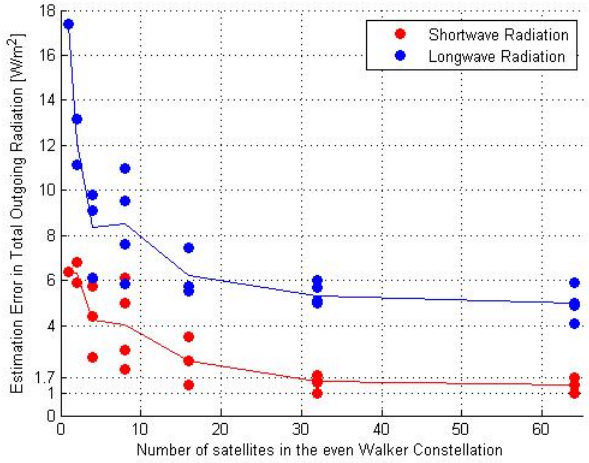

Figure 17: Norm-1 error of the TOR retrieved from simulated measurements by an N-satellite Walker constellation (710 km) using a 1D spherical harmonics model at the Equator and anisotropic TOR from UMGLO, corrected with CAR data.

Figure 17 shows that the saturated errors in Figure 11 and the increased errors due to anisotropy in Figure 16 can be improved significantly when SH is introduced. Not only are 50-80% improvement in errors seen compared to monoliths, the absolute errors are very

close to NOAA allowed uncertainties. While only the 1D model at the Equator has been used so far, since equatorial coverage and overlap is the worst, these values may be assumed representative.

Cost Results

The cost model described in the methodology, where RAVAN estimates are used to cost the TFU followed by cost to copy assessment to calculate subsequent costs, is used to calculate the cost of developing 1 through 64 satellites. The model is very simplistic in that it assumes that integration, launch and operations cost will scale up from RAVAN costs just as spacecraft development costs will. A learning curve parameter of 0.662, as computed for APL's business practices, is applied instead of the suggested 0.85 in the NASA Cost Engineering Handbook[34]. The results of the cost analysis are shown in Figure 18. Recurring costs per subsystem are currently not available, therefore an average recurring cost fraction is assumed to be between 40% to 60% of the total cost. For a low recurring cost (40%), the entire cost of the 64-satellite constellation fits within a typical Earth Venture Mission class budget and is able to achieve the required science goals. Lower number of satellites can also be easily evaluated in terms of the ratio of cost (Figure 18) to benefit (Figure 15 or Figure 16 or Figure 17).

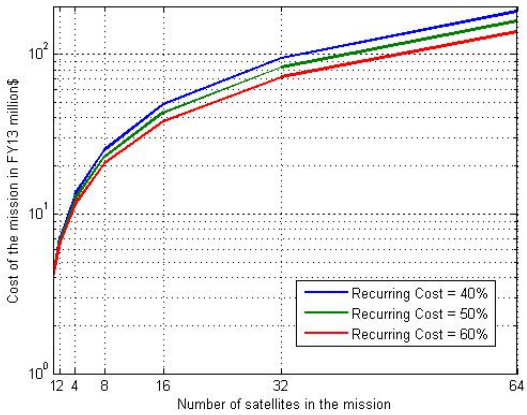

Figure 18: Cost to develop the constellation as a function of the number of satellites and recurring cost as a function of total cost.

CONCLUSIONS AND FUTURE WORK

An MBSE- and OSSE-based tradespace analysis tool has been developed for constellation mission design. The tool is based in MATLAB and STK and has a tightly coupled systems engineering and science evaluation model for iterative design that enumerates architectures by varying design variables using MBSE with the goal of reducing OSSE errors. To demonstrate the tool's utility, it has been applied to an Earth Radiation Budget Experiment (ERBE) and initial results have shown partial satisfaction of the science goals. Constellation design sensitivity to some key variables such as number of satellites, altitude, inclination, field of view, radiation anisotropy and science models has been demonstrated.

Future work includes using a very detailed 2D Spherical harmonics for flux estimation, as described in the methodology, and a full factorial study varying more design variables to assess its effect on ERB accuracy. A higher fidelity cost model with high resolution dependence on maintenance and launch costs also needs to be developed to evaluate Pareto optimality better. The full architecture enumeration and comparison will lead to the selection of the global Pareto optimal architectures, which can serve as candidates for a possible flight mission.

ACKNOWLEDGMENTS

I would like to thank Prof. Olivier de Weck and Dr. Daniel Selva at MIT; Warren Wiscombe, Shin-Chan Han, Jacqueline Lemoigne and Charles Gatebe at NASA GSFC, MD; Lars Dyrud at Draper Laboratory, MA; Christine Chiu at University of Reading, UK for sharing their prior work and for very useful discussions on the topic of research presented. The UMGLO model data has been obtained with permission via Christine Chiu, from Malcolm Brooks at the Met Office and Richard Allan at the University of Reading. This project has been funded by the Charles Stark Draper Laboratory, MA, and the Schlumberger Faculty for the Future Fellowship.

REFERENCES

1. O'Neill, M. G., Yue, H., Nag, S., Grogan, P. & de Weck, O. Comparing and Optimizing the DARPA System F6 Program Value-Centric Design Methodologies. in *Proceedings of the AIAA Space Conference* (2010).
2. De Weck, O. L., Neufville, R. D. & Chaize, M. Staged deployment of communications satellite constellations in low earth orbit. *Journal of Aerospace Computing, Information, and Communication* **1,** 119–136 (2004).
3. Wertz, J. R. *Orbit & Constellation Design & Management, second printing ed. El Segundo*. (California: Microcosm Press, 2009).
4. Nag, S. & Summerer, L. Behaviour based, autonomous and distributed scatter manoeuvres for satellite swarms. *Acta Astronautica* **82,** 95–109 (2013).
5. Nag, S. Collaborative competition for crowdsourcing spaceflight software and STEM education using SPHERES Zero Robotics. (2012).

6. Spangelo, S. C. *et al.* Applying model based systems engineering (MBSE) to a standard CubeSat. in *Aerospace Conference, 2012 IEEE* 1–20 (IEEE, 2012).
7. Loeb, N. G. *et al.* Toward optimal closure of the Earth's top-of-atmosphere radiation budget. *Journal of Climate* **22,** 748–766 (2009).
8. Loeb, N. G., Wielicki, B. A., Wong, T. & Parker, P. A. Impact of data gaps on satellite broadband radiation records. *Journal of Geophysical Research: Atmospheres (1984–2012)* **114,** (2009).
9. Trenberth, K. E. *et al.* Challenges of a sustained climate observing system. (2011).
10. Trenberth, K. E. & Fasullo, J. T. Tracking Earth's energy. *Science* **328,** 316–317 (2010).
11. Trenberth, K. E., Fasullo, J. T. & Kiehl, J. Earth's global energy budget. *Bulletin of the American Meteorological Society* **90,** 311–323 (2009).
12. Hansen, J. *et al.* Earth's energy imbalance: Confirmation and implications. *science* **308,** 1431–1435 (2005).
13. Wielicki, B. A. *et al.* Clouds and the Earth's Radiant Energy System (CERES): An earth observing system experiment. *Bulletin of the American Meteorological Society* **77,** 853–868 (1996).
14. Aires, F. & Rossow, W. B. Inferring instantaneous, multivariate and nonlinear sensitivities for the analysis of feedback processes in a dynamical system: Lorenz model case-study. *Quarterly Journal of the Royal Meteorological Society* **129,** 239–275 (2003).
15. Wielicki, B. A. & Harrison, E. F. Mission to planet Earth: Role of clouds and radiation in climate. *Bulletin of the American Meteorological Society* **76,** (1995).
16. Esper, J., Neeck, S., Wiscombe, W., Ryschkewitsch, M. et al. Leonardo-BRDF: A New Generation Satellite Constellation. (2000). at <http://ntrs.nasa.gov/search.jsp?R=20000105058>
17. Hughes, S. P. & Mailhe, L. M. A preliminary formation flying orbit dynamics analysis for Leonardo-BRDF. in *Aerospace Conference, 2001, IEEE Proceedings.* **2,** 2–579 (2001).
18. Dyrud, L. *et al.* GEOScan: A global, real-time geoscience facility. in *Aerospace Conference, 2013 IEEE* 1–13 (2013).
19. Dyrud, L. P. *et al.* Solving climate uncertainty one tiny satellite at a time: Earth's Radiation Imbalance System. in *AGU Fall Meeting Abstracts* **1,** 03 (2013).
20. Nag, S., Gatebe, C. K. & De Weck, O. L. Relative Trajectories for Multi-Angular Earth Observation using Science Performance Optimization. in *IEEE Xplore, Aerospace Conference 2014* (2014).
21. Nag, S. Design of Nano-satellite Cluster Formations for Bi-Directional Reflectance Distribution Function (BRDF) Estimations. *AIAA/USU Conference on Small Satellites* (2013).
22. Nag, S., LeMoigne, J. & De Weck, O. L. Cost and Risk Analysis of Small Satellite Constellations for Earth Observation. in *IEEE Xplore, Aerospace Conference 2014* (2014).
23. Gu, J. *et al.* Time-varying surface appearance: acquisition, modeling and rendering. in *ACM Transactions on Graphics (TOG)* **25,** 762–771 (2006).
24. Han, S.-C. & Ditmar, P. Localized spectral analysis of global satellite gravity fields for recovering time-variable mass redistributions. *Journal of Geodesy* **82,** 423–430 (2008).
25. Han, S.-C. *et al.* Non-isotropic filtering of GRACE temporal gravity for geophysical signal enhancement. *Geophysical Journal International* **163,** 18–25 (2005).
26. Gaposchkin, E. M. Averaging on the surface of a sphere. *Journal of Geophysical Research: Solid Earth (1978–2012)* **85,** 3187–3193 (1980).
27. Allan, R. P., Slingo, A., Milton, S. F. & Brooks, M. E. Evaluation of the Met Office global forecast model using Geostationary Earth Radiation Budget (GERB) data. *Q.J.R. Meteorol. Soc.* **133,** 1993–2010 (2007).
28. Lyapustin, A. *et al.* Analysis of snow bidirectional reflectance from ARCTAS Spring-2008 Campaign. *Atmos. Chem. Phys* **10,** 4359–4375 (2010).
29. Gatebe, C. K. Airborne spectral measurements of surface–atmosphere anisotropy for several surfaces and ecosystems over southern Africa. *Journal of Geophysical Research* **108,** (2003).
30. Hihn, J., Rosenberg, L., Roust, K. & Warfield, K. Cost model validation: a technical and cultural approach. (2001).
31. Warfield, K. & Roust, K. The JPL Advanced Projects Design Team's Spacecraft Instrument Cost Model: an Objective, Multivariate Approach. (1998).
32. Whitley, S., Hahn, M. & Powers, N. The Incremental Cost of One or More Copies–Quantifying Efficiencies from Building Spacecraft and Instrument Constellations. in *AIAA/USU Conference on Small Satellites* **52,** 31 (2013).
33. Apgar, H., Bearden, D. & Wong, R. Cost modeling. *Space Mission Analysis and Design, 3rd ed., El Segundo, Calif.: Microcosm Press and Kluwer Academic Publishers* (1999).
34. Shishko, R. & Aster, R. NASA systems engineering handbook. *NASA Special Publication* **6105,** (1995).